nature communications

Article

https://doi.org/10.1038/s41467-026-68427-y

Vegetation greening drives long-term dust mitigation in Eastern Asia

Received: 1 April 2025

Accepted: 7 January 2026

Published online: 27 January 2026

Check for updates

Yang Fu[1,2,3,4], Chenglai Wu[5,6], Shan Gao[2], Josep Peñuelas[3,4], J. Julio Camarero[7], Jingtian Zhang[2,3,4], Dou Li[2,8], Xiangyu Zheng[2,9], Zhuolun Li[1], Yafeng Wang[2] ✉, Eryuan Liang[2] & Shilong Piao[2,10]

Dryland vegetation dynamics play a fundamental role in dust mitigation. While weaker winds have driven recent dust decline in Eastern Asia, the long-term influence of vegetation remains overlooked. Here, using a physically based modeling approach that partitions the drivers of dust emissions across timescales, we reveal that surface wind dominates interannual variability, negatively correlated with the El Niño–Southern Oscillation, Arctic Oscillation, and Pacific Decadal Oscillation. On a multidecadal scale, however, vegetation cover emerges as the key driver, reducing dust emissions by 32.5% since the early 2000s—a trend projected to continue through 2100. Without these vegetation gains, dust emissions would increase under various CMIP6 projections. Vegetation contributions are uneven: greening of perennial dryland vegetation in sparsely vegetated regions (<15% cover; responsible for 95% of dust emissions) offers the greatest mitigation by stabilizing the land surface and suppressing long-term emissions. These findings highlight priority areas for ecological restoration to sustain dust reduction and advance regional sustainability goals.

Sand and dust storms (SDS) release up to 2 billion tonnes of dust annually, affecting over 150 countries[1] and posing serious health risks, including excess mortality[2,3]. These emissions from drylands have substantial impacts on climate and public health, and are further amplified by ecological degradation and land mismanagement[4–7]. Although both climate variability and land surface changes, particularly changes in vegetation cover, are recognized as major drivers of dust activity across global drylands[5,8–11], surprisingly, their relative contributions to dust variability remain unclear. Substantial vegetation changes have been observed in drylands[12], but their effects on dust activity remain highly heterogeneous because wind merely triggers emissions from surfaces whose susceptibility is modulated by vegetation[13–15]. Disentangling the relative influence of land surface processes and atmospheric drivers is therefore critical to understanding dust emission variability and informing large-scale land management strategies.

Dust emissions are often examined within distinct disciplinary frameworks[16]: paleoenvironmental and sedimentary studies tend to emphasize long-term changes in surface conditions, such as vegetation cover and soil erodibility (i.e., how easily mineral particles can be picked up and transported by wind), which are influenced by climatic trends over decades to centuries[17,18]; while meteorological analyses

[1]College of Earth and Environmental Sciences, Lanzhou University, Lanzhou, Gansu, China. [2]State Key Laboratory of Tibetan Plateau Earth System, Environment and Resources (TPESER), Institute of Tibetan Plateau Research, Chinese Academy of Sciences, Beijing, China. [3]CREAF, Cerdanyola del Valles, Barcelona, Catalonia, Spain. [4]CSIC, Global Ecology Unit CREAF-CSIC-UAB, Bellaterra, Barcelona, Catalonia, Spain. [5]State Key Laboratory of Earth System Numerical Modeling and Application, Institute of Atmospheric Physics, Chinese Academy of Sciences, Beijing, China. [6]International Center for Climate and Environment Sciences, Institute of Atmospheric Physics, Chinese Academy of Sciences, Beijing, China. [7]Instituto Pirenaico de Ecología (IPE-CSIC), Zaragoza, Spain. [8]College of Ecology, Lanzhou University, Lanzhou, Gansu, China. [9]University of Chinese Academy of Sciences, Beijing, China. [10]Institute of Carbon Neutrality, Sino-French Institute for Earth System Science, College of Urban and Environmental Sciences, Peking University, Beijing, China. ✉e-mail: yfwang@itpcas.ac.cn

typically focus on interannual variability, often by analyzing specific years or extreme events driven by surface winds, droughts, and large-scale circulation patterns[8,19,20]. This difference between disciplinary perspectives has led to a fragmented understanding of how dust interacts with land and climate across timescales and disciplines. For example, in the Sahel, dust activity rose sharply in the 19th century, coinciding with both drying trends and agricultural expansion[21]. Similarly, historical records from China show increased dust storms during times of population growth and land use intensification under strong monsoon climates[22]. These long-term perspectives can complement recent studies that emphasize the role of meteorological factors, such as wind weakening[23], in shaping dust trends during 2001–2017, and together highlight the need for a multidisciplinary, scale-dependent understanding of dust–climate–land interactions. These contrasting findings raise a central question: to what extent are dust emission dynamics governed by different drivers across temporal scales?

Despite increasing recognition that dust-generating processes operate across multiple timescales, few studies have explicitly quantified how the relative importance of vegetation and climate drivers varies with frequency. Eastern Asia presents a particularly compelling case study. On the one hand, both afforestation and land stabilization efforts, such as China's Three-North Shelterbelt Program, and declining surface wind speeds have been associated with reduced dust activity in recent decades[23,24]. On the other hand, severe dust outbreaks, including those in 2021 and 2023 that blanketed northern China and Mongolia (Supplementary Fig. 1)[19,25], continue to emerge episodically, raising public concern over the long-term effectiveness of these programs[19]. This apparent contradiction underscores the need to reconcile long-term ecological trajectories with high-frequency climatic variability. However, a comprehensive evaluation of dust drivers remains lacking, both in Eastern Asia and globally.

To disentangle the temporal dynamics of dust variability in Eastern Asia, we developed a timescale-explicit framework to quantify the relative contributions of vegetation and climate drivers (see Supplementary Fig. 2 for an overview). This framework integrates physically based modeling with statistical attribution to assess dust mitigation by vegetation across historical (1982–2023) and future (2015–2100, CMIP6) periods. Dust emissions are analyzed across multiple spatial scales (land uses, ecoregions) to inform targeted mitigation policies. Our study focuses on springtime dust emissions from the Gobi Desert and surrounding regions because (1) it is the primary source of dust affecting densely populated regions in Eastern Asia (Fig. 1a, b, Supplementary Fig. 3a and Methods); (2) dust emissions in this region

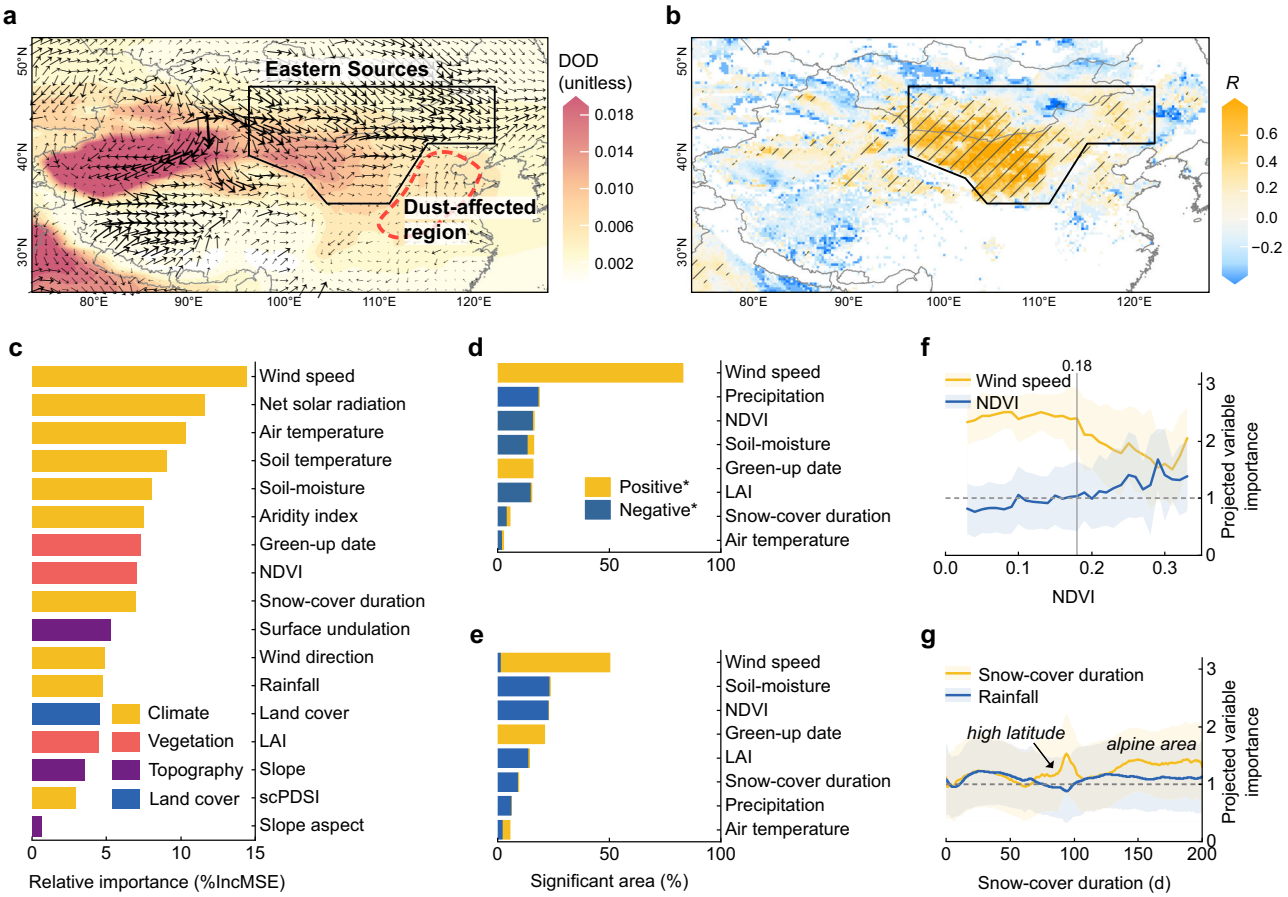

Fig. 1 | Patterns and statistical attributions of dust activity in Eastern Asia. **a** Spatial pattern of mean spring (March–May) MERRA-2 dust optical depth (DOD, dimensionless), with arrows indicating mean wind speed and direction; arrow length is proportional to wind speed. The black polygon indicates Eastern Sources. **b** Pearson correlations linking downwind DOD to source-region dust emissions simulated by DuEM v1, with significant areas hatched ($P < 0.05$). **c** Variable importance (%IncMSE: percent increase in mean squared error) in predicting spatial dust emission using the random forest method. Partial correlations of key factors within the Eastern Sources with dust emissions (**d**) and downwind DOD (**e**) (* $P < 0.05$). Importance of key factors on normalized difference vegetation index (NDVI) (**f**) and snow-cover duration (**g**) from the partial least-squares regression (PLSR) model. Solid lines and shaded areas show mean and standard deviation. The gray line represents the inflection point of variable importance detected by the Change Point Analysis v1.20 tool in OriginPro 2024. The dashed gray horizontal line indicates the level of significance of the variable importance in the PLSR model, typically set at one. Basemaps in **a** and **b** from Natural Earth (https://www.naturalearthdata.com/).

exhibit strong seasonal variability, with peaks in spring (March–May), dominating annual dust activity (Supplementary Figs. 4 and 5); and (3) dust activity is strongly negatively correlated with vegetation greenness (Supplementary Fig. 4), highlighting the regulatory role of vegetation in dust mitigation.

Results and discussion

Climate-driven intra- and interannual dust variability

Dust emissions from Eastern Asia are profoundly influenced by surface wind across the region. As shown by the random-forest algorithm (Fig. 1c), surface wind speed (at a height of 10 m), climatic variables (net solar radiation, air temperature, soil temperature, soil moisture, Aridity Index) and vegetation (green-up date and Normalized Difference Vegetation Index (NDVI)) explained 15%, 8–12%, and 7% of the variance in dust emission, respectively. Similarly, surface wind speed, NDVI, and moisture availability (precipitation or soil moisture) ranked among the strongest drivers of dust emissions in the partial correlation analysis (Fig. 1d, e and Supplementary Fig. 6). The effects of wind speed were particularly pronounced in areas with sparse vegetation and low soil moisture, characterized by erodible surface conditions (Supplementary Fig. 6i).

The climate impacts on dust emissions strongly interact with surface conditions, reflecting spatial heterogeneity in land–atmosphere coupling. The partial least-squares regression model revealed that the variable importance projection (VIP) for key factors is strongly contingent on vegetation biomass and the duration of snow cover (Fig. 1f, g). For example, VIP_{Wind} decreased sharply as vegetation biomass increased when the mean NDVI was > 0.18. By contrast, VIP_{NDVI} increased and eventually surpassed VIP_{Wind} when the mean NDVI reached a threshold of 0.3. Both snow-cover duration and spring rainfall contributed regionally to dust variability, with snow duration exerting stronger control than rainfall in high-latitude and alpine regions (Fig. 1g).

Strong surface winds in Eastern Asia are primarily driven by large-scale circulation systems, including the Mongolian Cyclone, the Siberian High, and synoptic-scale low-pressure troughs[8,23]. We suggest that these patterns are closely linked to broader climate modes, particularly the El Niño-Southern Oscillation (ENSO), Pacific Decadal Oscillation (PDO), North Atlantic Oscillation (NAO), and Arctic Oscillation (AO) (Supplementary Fig. 7). During La Niña events, surface winds over northern China and Mongolia strengthen[26], and this linkage may be further amplified during the negative phase of the PDO[27]. We further demonstrate that the PDO can predict dust intensity in Eastern Asia up to six months in advance, even earlier than the Niño 3.4 index (Supplementary Fig. 7a). Additionally, negative phases of the NAO and AO weaken the polar vortex, allowing cold Arctic air to move southward[28]. This strengthens the Siberian High and intensifies the Mongolian Cyclone, leading to more frequent and intense dust storms in the region. These findings underscore the complex interactions between large-scale atmospheric circulation patterns and dust emission in Eastern Asia.

Vegetation contributions to dust emissions (1982–2023)

Our model captures observed variability in dust activity, as indicated by significant correlations with MERRA-2 DOD ($R^2 = 0.53–0.67$, $P < 0.001$) and with observed dust storm days ($R^2 = 0.44–0.55$, $P < 0.001$; Supplementary Fig. 8). Simulated dust emissions in the Eastern Sources exhibited a non-monotonic trend—first increasing and then declining over the past four decades (Fig. 2e). Spatially, however, large areas of the Mongolian Plateau continued to experience increasing emissions during 2001–2023 (Fig. 2a, b). To understand the drivers behind these patterns, we identified four primary factors—surface wind speed, vegetation cover, soil moisture, and snow cover—and analyzed their relative contributions using model simulations over the entire study period. This analysis incorporated data from both GIMMS (1982–2015) and MODIS (2001–2023) (Experiment 1, Supplementary Table 1; see Methods). The overlapping interval (2001–2015) represents a high-emission plateau during a transition phase, and is used primarily for cross-validation and consistency in trend attribution, without implying independent or conflicting trends.

Increasing dust emissions from 1982 to around 2000 were primarily driven by enhanced surface wind speeds (+2.1 g m^{-2} $decade^{-1}$, $P < 0.01$), with additional contributions from reduced soil moisture in specific regions (+0.2 g m^{-2} $decade^{-1}$) (Fig. 2c). During the same period, vegetation changes also contributed positively to dust emissions: browning over the Mongolian grassland (steppe) (~6% of the area, $P < 0.05$) exceeded modest greening in surrounding regions (~3%, $P < 0.05$) (Supplementary Fig. 9b, e), resulting in a small net increase in dust emissions (+0.03 g m^{-2} $decade^{-1}$). Together, these factors resulted in a net increase of +2.4 g m^{-2} $decade^{-1}$ in dust emissions across the Eastern Sources (Fig. 2a).

In contrast, dust emissions decreased (−4.4 g m^{-2} $decade^{-1}$) from 2001 to 2023 (Fig. 2b), mostly due to lower wind speeds and higher vegetation cover (Supplementary Fig. 9). Wind-driven dust emissions decreased across the Eastern Sources by 4.9 g m^{-2} $decade^{-1}$, especially for the main sources of dust in northwestern Inner Mongolia (Fig. 2d). Vegetation cover further reduced dust emissions in the same area (−1.5 g m^{-2} $decade^{-1}$, $P < 0.001$). By contrast, the drying of topsoil across Mongolia's dust sources has led to an increase in dust emissions (+2.0 g m^{-2} $decade^{-1}$, $P < 0.05$). Snow cover regionally influenced dust emissions, with effects mainly limited to southern Mongolia and the western Tibetan Plateau, where snow cover lasts longer (Supplementary Fig. 10).

The role of vegetation in dust emission was further validated by an additional experiment (Experiment 2, Supplementary Table 1), comparing scenarios with vegetation fixed at its initial-year state versus fully time-varying vegetation cover. Including time-varying vegetation cover improved the model's ability to reproduce observed dust storm days in downwind regions, with R^2 increasing from 0.50 to 0.55 ($P < 0.001$, Supplementary Fig. 8). This finding aligns with Fig. 2e, f, where vegetation-driven reductions in dust emissions became more pronounced after 2000. Specifically, Theil–Sen slopes indicate a 32.5% reduction in dust emissions relative to the fixed-vegetation experiment, consistent with the intensified greening trend in Eastern Sources (Supplementary Fig. 9e). The rolling correlation analysis (Supplementary Fig. 11b) indicates a shift that began in the early 2000s: vegetation became more strongly linked to reductions in DOD, while the influence of wind declined. Separately, vegetation seemed increasingly disconnected from soil moisture and rainfall (Supplementary Fig. 11a), suggesting that other factors—such as CO_2 fertilization or ecological restoration—may have played an increasingly significant role.

Vegetation cover increased significantly from 2001 to 2023 across barren land, grassland, and cropland ($P < 0.001$), with mean FVC increases of ~0.3, ~1.4, and ~1.7 per decade, respectively, leading to reduced dust emissions (Supplementary Fig. 12). A substantial area of barren land ($7.4–10.7 \times 10^4$ km^2; Supplementary Fig. 12a–d) was converted to grasslands over the past three decades. The ongoing greening of desert and steppe ecosystems in the Alashan Plateau, eastern Gobi Desert, and Ordos Plateau have greatly contributed to the decrease in dust emissions (Supplementary Fig. 13a–d). Notably, more than 70% of regionally accumulated dust originates from the Alashan Plateau, which only covers 30% of the Eastern Sources. This region is dominated by xerophytic desert vegetation composed mainly of perennial woody and semi-woody shrubs such as *Reaumuria soongarica*, *Artemisia salsoloides*, *and Calligonum mongolicum* (see Supplementary Table 2 for additional dominant vegetation types). The deep and persistent root systems of these xerophytic shrubs act as ecological stabilizers, reinforcing surface soil structure and mitigating erosion despite their sparse aboveground cover[29]. In

https://doi.org/10.1038/s41467-026-68427-y

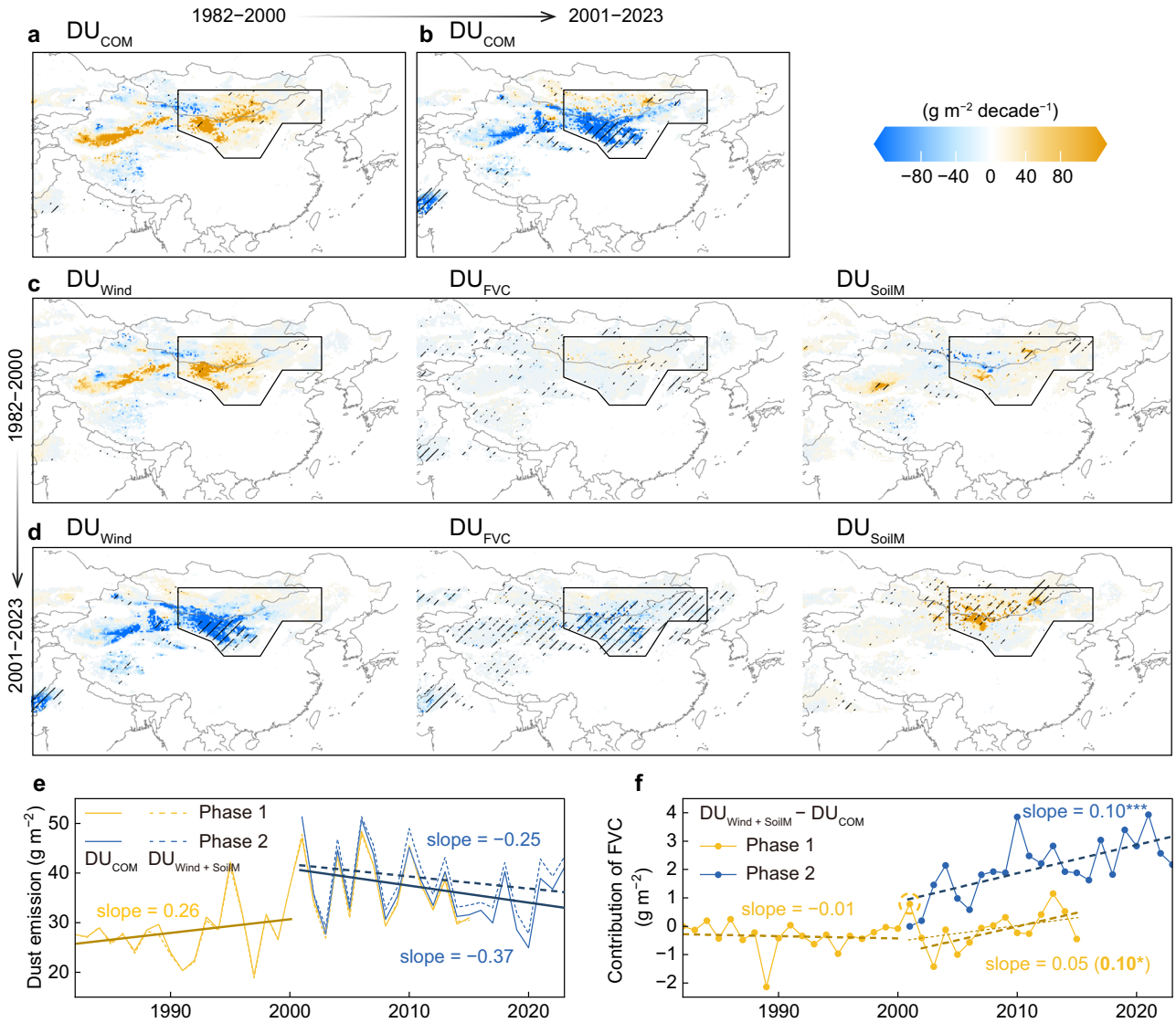

Fig. 2 | The contributions of drivers to dust variations in Eastern Asia during two historical phases. a, **b** Theil–Sen trend estimates of modeled dust time series from 1982 to 2000 and from 2001 to 2023; diagonal lines denote trends significant at $P < 0.05$. **c**, **d** Theil–Sen trends in dust emissions attributed to individual drivers for two periods: 1982–2000 and 2001–2023 (Experiment 1; Supplementary Table 1). **e** Time series of simulated dust emissions under baseline (solid) and fixed-vegetation (dashed) conditions from 1982 to 2023 (Experiment 2). Yellow lines: simulations driven by GIMMS fractional vegetation cover (FVC) (Phase 1); blue lines: simulations driven by MODIS FVC (Phase 2). **f** Difference between the two scenarios shown in (**e**), showing an increasing vegetation contribution after 2000. The dashed circle marks an outlier (2001) within 2001–2015; the bold number in parentheses indicates the slope after its exclusion. * $P < 0.05$; *** $P < 0.001$. Basemaps in **a**–**d** from Natural Earth (https://www.naturalearthdata.com/).

contrast, the remaining four ecoregions are dominated by perennial grasses and semi-arid steppe vegetation characteristic of the Mongolian Plateau, and contribute relatively little to dust emissions. Nevertheless, observed water limitations in our study domain (Supplementary Fig. 13e–g), consistent with global patterns[30], combined with increased grazing pressure, may pose unexpected risks in the absence of adequate management.

Threshold-dependent effects of vegetation on dust mitigation

The path model for the interannual variability in dust activity reveals that wind speed exerts the strongest direct effect (Supplementary Fig. 14a, b). Our model experiments show that surface wind (80.7%) and vegetation cover (20.11%) account for most of the modeled change in dust emissions from 2001 to 2017, based on their isolated contributions relative to 2001 baseline conditions (Fig. 3a–c; Experiment 3; Supplementary Table 1), supporting previous findings[23]. Vegetation also indirectly affects dust emissions through its modification of surface conditions, which in turn alter near-surface wind dynamics and soil-moisture availability (Supplementary Fig. 14c).

Spatial analyses reveal pronounced heterogeneity in the response of dust emissions to vegetation changes (Fig. 3). This pattern arises from a critical vegetation threshold, beyond which bottom-up factors (e.g., vegetation cover and surface roughness) limit the effectiveness of top-down drivers (e.g., wind speed) in generating dust emissions. Over 95% of dust emissions originate from regions where the spring fractional vegetation cover (FVC), averaged over 2001–2023 from MOD13C1, is below 15% (Fig. 3b). Beyond this threshold, dust emissions become significantly less sensitive to wind speed. The robustness of this threshold arises from interactions among different biomes, plant morphologies, and soil properties[31] (Supplementary Figs. 15–16). Near this threshold, grassland dynamics—such as expansion, contraction, or shrub encroachment—imply potential changes within the sub-threshold range (Supplementary Fig. 17) and play a key role in modulating dust emission responses. Observed increases in grassland area

https://doi.org/10.1038/s41467-026-68427-y

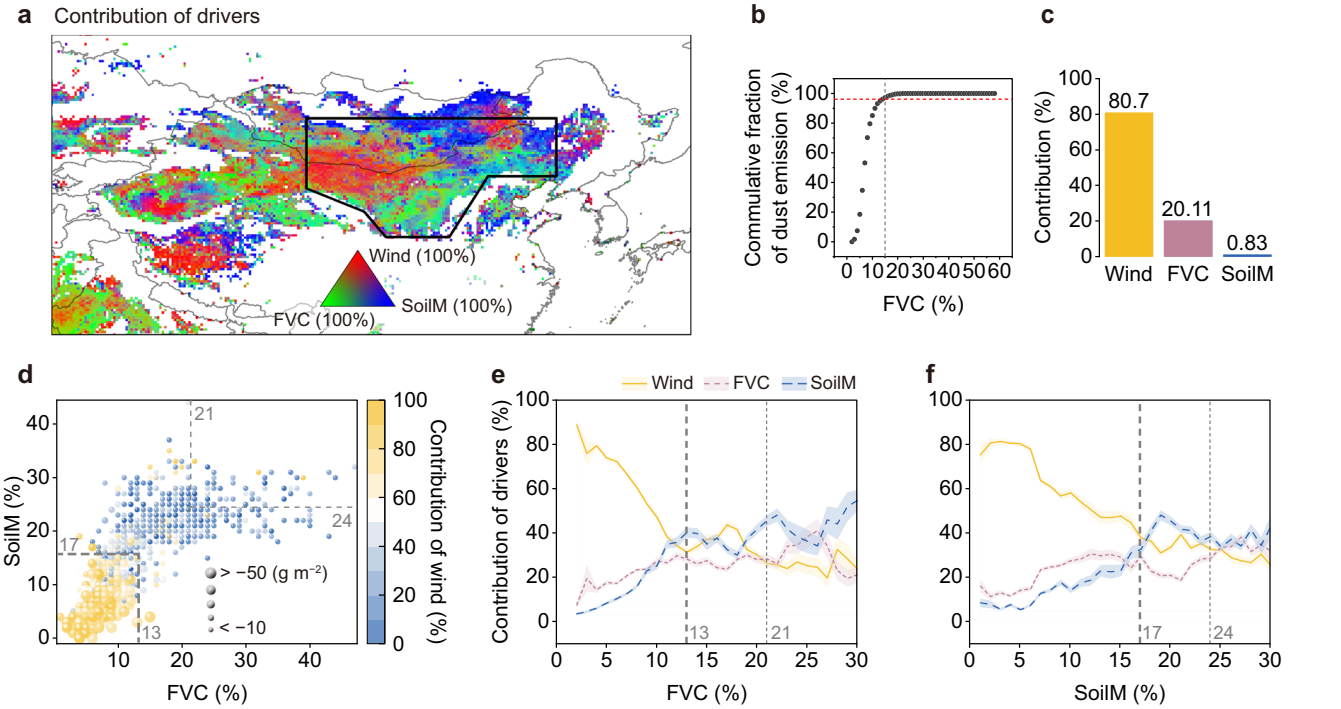

Fig. 3 | Contributions of drivers to dust anomalies during the historical period and their dependencies across fractional vegetation cover (FVC) and soil moisture (SoilM). a Spatial distribution of percent contributions of three factors (Wind, FVC, and SoilM); dominant factor per pixel is indicated. **b** Cumulative mean dust emissions (1982–2023) along the FVC gradient. Black and red dashed lines denote the FVC threshold (15%) and the corresponding cumulative fraction (96.19%), respectively. **c** Absolute percent contributions of the three factors in the Eastern Sources (Experiment 3). **d** The constraints of FVC and SoilM on wind-driven dust. The sizes of the spheres represent the dust anomalies induced by wind. The thick dashed lines represent the values of FVC and SoilM corresponding to a wind contribution of 95%. The thin dashed line represents the values of FVC and SoilM corresponding to the 95th percentile of pixel values of wind-driven dust emissions. **e**, **f** The dependence of the contributions of the three factors on FVC and SoilM. Shaded areas represent the standard deviation estimated via bootstrap resampling (500 iterations). Basemap in **a** from Natural Earth (https://www.naturalearthdata.com/).

and FVC over bare soil may enhance surface stabilization and suppress dust emissions (Supplementary Figs. 12 and 17c–f). Ecoregions within this sub-threshold zone, including the Alashan Plateau, warrant particular attention, as any reduction in FVC there cannot be offset by improvements elsewhere. Identifying these threshold-dependent effects is crucial for optimizing dust mitigation strategies.

Multidecadal declines in dust emissions in a greener world

Pronounced interannual fluctuations in dust emissions are closely aligned with wind-driven components of simulations under various Shared Socioeconomic Pathways (SSP1-2.6, SSP2-4.5, SSP5-8.5) in CMIP6, particularly in high-frequency patterns (Fig. 4a–c). However, when short-term fluctuations are excluded (dashed boxes in Fig. 4d), vegetation cover shows the strongest correlation with dust emissions over long-term (multidecadal) scales across all scenarios. This shift in dominant drivers is further supported by EEMD-based timescale decomposition (Supplementary Fig. 18), which reveals that wind signals dominate at shorter timescales (e.g., IMF1–IMF3), while perennial vegetation within dust source regions emerges as the leading driver at longer timescales (IMF4 and above). This pattern primarily reflects the influence of perennial, sparsely distributed vegetation within areas of FVC below ~15%, where dust emissions are most sensitive to change.

Dust emissions in future climate scenarios are projected to decrease by the end of the 21st century compared to the period 2015–2035 (Fig. 4 and Supplementary Fig. 19), largely due to increases in vegetation cover (Supplementary Fig. 20). Notably, the greatest reduction occurs under the scenario with the most substantial vegetation greening. Specifically, under SSP2-4.5 and SSP5-8.5, rising vegetation cover is expected to reduce dust emissions by 47% and 64%, respectively (black line in Fig. 4b, c). However, if vegetation remains constant without further greening, dust emissions would stabilize or even increase (purple line in Fig. 4b, c).

As vegetation cover increases, its role in mitigating dust emissions enhances over time (gray bars in Fig. 4a–c). We predict that, despite stable soil-moisture content (Supplementary Fig. 20c), dust emissions will consistently decrease from the late 2050 s to the early 2080 s (Fig. 4c), given that the positive effect of vegetation cover outweighs the negative effects of increased surface wind speed. Vegetation resilience, particularly of perennial woody and semi-woody shrubs in desert regions (e.g., the Alashan Plateau) and perennial grasses in semi-arid steppe regions (e.g., the Mongolian Grassland), underpins the multi-year mean vegetation status and essential ecosystem services[32], hence buffering against short-term fluctuations in dust emissions. Regional greening in China's drylands over past decades has been attributed to favorable climate conditions, CO_2 fertilization, and land-use optimization[33–36], and is projected to continue within dust source regions under future climate scenarios (Supplementary Fig. 20). Separate projections indicate that China's dryland extent, defined as regions with an Aridity Index below 0.5, may decline by 9.3%, 13.4%, and 17.3% by 2050, 2070, and 2100, respectively[37]. These trends support our predictions and underscore the potential of gradual desert contraction to mitigate dust emissions.

Implications for dust mitigation and land management policies

Our analysis reveals that dust activity arises not merely from short-term fluctuations, but from long-term trajectories shaped by slowly evolving environmental drivers. Over the past four decades, dust emissions have exhibited a non-monotonic trend, characterized by an initial increase followed by a subsequent decline, driven by the combined influences of vegetation, wind speed, and soil moisture.

https://doi.org/10.1038/s41467-026-68427-y

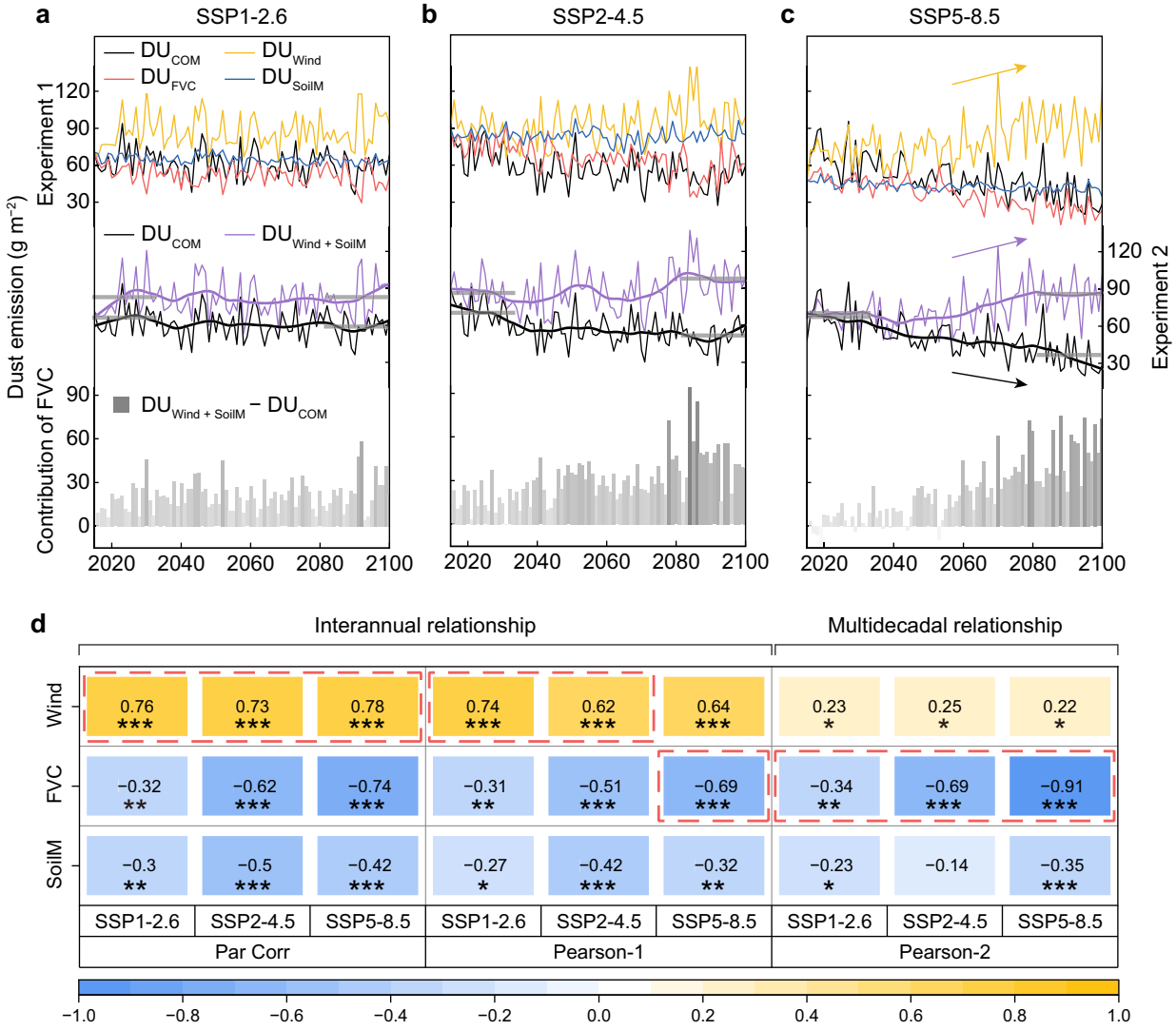

Fig. 4 | Variations in dust emissions and the contributions of drivers under the Coupled Model Intercomparison Project Phase 6 (CMIP6) scenarios. a–c The dust-emission time series in the CMIP6 scenarios obtained from two types of experiments (the first and second rows of columns; Supplementary Table 1), and the contributions of vegetation cover (FVC) to dust calculated from Experiment 2 (the third row of columns). The thick line represents the locally estimated scatterplot smoothing (LOESS) smoothing. The bold horizontal lines flanking the columns represent the means of dust emission in the preceding and succeeding two decades, serving as indicators of the magnitudes of the dust anomalies. **d** Relationships between drivers and predicted dust emission. Partial correlation analysis (Par Corr) was used to calculate the partial correlation coefficient between each factor and the original model output, controlling for the other two factors. Pearson-1 represents the Pearson correlation between the factors and the original model output. Pearson-2 is similar to Pearson-1, but the simulated dust emission was subjected to a twenty-year window Savitzky-Golay filter to represent its trend component. The dashed boxes represent the dominant factors driving the two types of dust variations. * $P < 0.05$; ** $P < 0.01$; *** $P < 0.001$.

Ensemble experiments integrating historical observations with CMIP6 scenario simulations indicate that vegetation increasingly mitigates dust emissions over multi-decadal timescales, largely driven by greening of perennial woody and semi-woody vegetation in key dust source regions, including xerophytic deserts such as those in the Alashan Plateau. By contrast, short-term fluctuations in dust emissions are primarily driven by interannual variations in vegetation cover and wind conditions. These results underscore that robust quantification of the long-term influence of vegetation on dust emissions requires extended observations and careful timescale separation; otherwise, the influence of slowly evolving environmental drivers on multi-decadal dust trends could be overlooked.

Vegetation interacts with other bottom-up drivers to shape land surface erodibility. Dry topsoil weakens the compactness of soil aggregates, making them more susceptible to erosion. Low soil moisture followed by delayed rainy season can also reduce vegetation activities over time by triggering partial stomatal closure[38–40]. Meanwhile, reduced surface air humidity can facilitate the emission of finer particulates through the adhesion process[41]. In cold regions, such as the northern Mongolian Plateau, early snowmelt in warm spring can expose the topsoil, offsetting the positive effects of early monsoon and green-up date on dust emissions[20,42]. These findings inform the complex impacts of surface conditions on dust and their implications for land management.

Feedbacks between vegetation and dust emissions in drylands are shaped by interactions among climate fluctuations, human interventions, and intrinsic vegetation traits. In Mongolian grasslands, persistent severe droughts which are regionally associated with elevated

dust emissions (Fig. 2), have constrained vegetation growth[43–45], thereby amplifying a positive feedback between vegetation browning and dust generation[46]. However, this negative trend can be mitigated through targeted human interventions[47], such as China's Grain for Green program. Initiated around 2000 to restore perennial vegetation in desertification-prone regions of northern China that overlap with parts of the dust sources considered in this study, this program has reduced wind erosion and associated dust emissions[48]. Despite declining water availability, the Eastern Sources as a whole have experienced increasing vegetation greenness, indicating a decoupling between vegetation dynamics and immediate water supply (Supplementary Fig. 11a), likely driven by improved water-use efficiency through reduced stomatal conductance[49]. These findings underscore the importance of considering human interventions, climatic forces, and vegetation physiology together when evaluating dust variability and designing mitigation strategies, particularly for xerophytic herbaceous and shrub communities that stabilize soils against wind erosion.

Socioeconomic changes have dramatically altered the functions and services of dryland ecosystems[12,24,50]. Drivers such as wind and solar energy development and rural-urban migration can indirectly affect natural vegetation recovery[51–53]. Recent rural depopulation in Eastern Sources may enhance vegetation greening (Supplementary Fig. 3), benefiting dust control and potentially becoming a significant future driver. Urban expansion in association with reducing cropland may not always hinder dust control, as impervious surfaces and optimized agricultural practices help minimize the exposure of erodible soil[54,55]. Consequently, substantial regional greening and associated land cover changes over the past decades largely explains the notable reductions in dust emissions (Supplementary Fig. 12e–g).

Based on our findings, we propose three principles to help reduce dust emissions and their potential impacts in Eastern Asia:

1. Forward-looking principle: Developing a deep understanding of slowly evolving land surface conditions[56], particularly changes in vegetation cover of dust sources, is essential. The long-term impact of vegetation dynamics is evidenced by our comparison between greening and no-greening scenarios (e.g., Figs. 2e and 4), as well as regional and vegetation-type differences in FVC effects, suggesting that vegetation greening, whether natural or human-facilitated, increasingly reduces dust emissions over multi-decadal timescales.
2. Threshold principle: Identifying both chronic and acute dust sources. In regions with sparse vegetation (below ~15% cover), even small increases in vegetation cover can yield substantial mitigation benefits, whereas beyond this threshold, benefits tend to saturate; thus, intervention costs rise disproportionately as the area of restoration expands. These effects also depend on vegetation type, since the benefits arise not only from coverage but also from other vegetation characteristics. Notably, this threshold serves as an operational guideline rather than a strict restoration target. In areas where vegetation recovery is unfeasible, alternative measures such as soil stabilization and windbreaks can be implemented to achieve similar dust reduction effects.
3. Key-role principle: Prioritizing ecoregions that exert disproportionate influence on dust emissions. For example, the steppes of the Alashan Plateau and the adjacent eastern Gobi Desert have had strong associations with regional dust trends. Our findings further indicate that April—the peak month for spring dust events—contributed most to the reduction in emissions from 2001 to 2017 (Supplementary Fig. 21). This highlights the importance of integrating both spatial and temporal processes when developing effective dust mitigation strategies. These actions are aligned with the forward-looking principle, emphasizing that sustainable development depends on common but differentiated Sustainable Development Goals rather than short-term regional gains[57].

This study acknowledges several uncertainties and limitations regarding data and model assumptions. First, surface winds, vegetation, and soil moisture are interdependent, and part of the interannual variability in wind or soil moisture may itself be vegetation-driven[23]. Although controlled model experiments were designed to isolate the effects of individual factors, they did not include explicit dynamic coupling among variables. Consequently, feedbacks such as vegetation-induced modification of near-surface winds or soil moisture persistence could not be fully represented, leaving the net vegetation effect uncertain. Second, this study primarily considers the effects of green vegetation, whereas the influence of dry or senescent vegetation—especially critical in regions where strong winds prevail outside the growing season—remains insufficiently constrained. Recent field surveys and satellite-based analyses have demonstrated that shortwave infrared (SWIR) indices, such as the MODIS Soil Tillage Index (STI), can reliably estimate dry vegetation coverage and its control on surface roughness and threshold friction velocity in arid regions[58,59]. Incorporating such STI-based estimates into future analyses would help quantify the mitigating role of dry vegetation in dust emission and narrow the current uncertainties associated with wind–vegetation interactions[59]. A more detailed discussion of these and other methodological issues is provided in the Supplementary Notes.

Overall, this study provides important support and nuanced insights to guide dust control policies in Eastern Asia. Our analysis helps to clarify the long-term (interdecadal or even longer) influence of vegetation cover on dust variability, which is often masked by atmospheric fluctuations. By offering process-based evidence across multiple timescales, our findings reveal that the benefits of vegetation greening, particularly for perennial dryland vegetation in dust source regions, become increasingly pronounced over longer periods, in conjunction with changes in wind speed. Moreover, conventional metrics that apply uniform vegetation interventions across regions fail to account for the spatially varying contributions of vegetation to dust emissions. We recommend prioritizing efforts to enhance vegetation in areas where cover is below 15%. Additionally, improving our understanding of the interactions between vegetation cover and dust emissions is crucial for enhancing the predictive power of Earth system models. Integrating these findings into policy frameworks will help develop targeted strategies to address both climate change and dust emissions, supporting more sustainable and informed land management practices.

Methods

Data sets of dust emission and determining the Eastern Sources

Monthly dust emission and dust optical depth (DOD), with spatial resolutions of 0.625 × 0.5°, were obtained from the tavgM_2d_adg_Nx data set in Modern-Era Retrospective Analysis for Research and Applications, version 2 (MERRA-2) (https://disc.gsfc.nasa.gov/datasets/M2TMNXADG_5.12.4/summary). We used MERRA-2 dust emissions for statistical attribution of driving factors and for comparison with output of another physically-based dust emission model, DuEM v1 (details in later sections). MERRA-2 DOD at 550 nm was derived from the variable of "Dust Extinction AOT (aerosol optical thickness)". Both satellite- and ground-based data for aerosol optical depth were assimilated to improve the distribution of aerosols in MERRA-2[60,61]. Therefore, we used MERRA-2 DOD to represent the dependent variable in statistical analysis.

Uncertainties in MERRA-2 DOD data stem from the evolving quality and availability of assimilated observational inputs over time. These include AVHRR (1980–2002), AERONET (1999–2014), MISR (2000–2014), MODIS Terra (2000 onward), and MODIS Aqua (2002 onward)[61]. For example, MERRA-2 may show discrepancies in regions such as the Taklamakan Desert, where sparse ground observations and

regional differences in data assimilation reduce the accuracy of DOD estimates[62]. To address these potential biases, we incorporated independent ground-based observations to validate the dust emission simulations. Specifically, we used springtime (March–May) dust storm day records from five WMO meteorological stations downwind in northern China spanning 2001–2023 (locations shown in Supplementary Fig. 8a; metadata in Supplementary Tables 3 and 4). These records provide an observational benchmark for assessing model performance beyond assimilated datasets, as dust storm day observations from WMO meteorological stations are not assimilated into the MERRA-2 aerosol reanalysis.

As shown in Supplementary Fig. 8c–d, DuEM outputs demonstrate strong agreement with both MERRA-2 DOD ($R^2 = 0.67$) and WMO meteorological station observations ($R^2 = 0.55$) after 2001. This dual validation enhances confidence in the reliability of MERRA-2 DOD and confirms its consistency with independent surface-based data. Moreover, although MERRA-2 data prior to 2000 may be less certain due to the limited availability of high-quality observational data for assimilation[61], the strong consistency between DuEM simulations driven by GIMMS and MODIS vegetation datasets during their overlapping period (2001–2015) (Supplementary Fig. 8c) indicates that the simulated dust emissions are robust to the choice of vegetation input, thereby increasing confidence in the modeled vegetation–dust relationships across the full study period.

Additionally, we employed monthly average dust storm days during 2001–2017 within the Eastern Sources region (35–49°N, 94–126.5°E), derived from Wu et al.[23]. This dataset, based on 339 synoptic stations reporting at least one dust storm day, provides an additional proxy for evaluating model performance at the regional scale (Supplementary Fig. 8d).

Given the strong spatial heterogeneity of dust emissions, accurately identifying source regions is essential for quantitative analysis. Based on the correlation between springtime simulated dust emissions and downwind aerosol loading (Fig. 1b), we delineated the Eastern Sources region (35–47°N, 96–122°E; Fig. 1a). Specifically, we calculated the Pearson correlation between spring (March–May) DuEM-simulated emissions at each grid cell and the area-averaged MERRA-2 DOD over the Beijing–Tianjin–Hebei (BTH) region—the most affected downwind area in the North China Plain (red dashed polygon in Fig. 1a). Grid cells showing significantly positive correlations ($P < 0.05$) were classified as part of the Eastern Sources. This method captures the dominant upwind–downwind transport relationships and reflects the underlying physical causality[63]. Notably, the identified region aligns with the prevailing northwesterly winds during spring (Fig. 1a). The resulting Eastern Sources are largely consistent with those defined by Wu et al.[23]. However, unlike Wu et al.[23], we excluded the North China Plain from the source region and instead treated it as a receptor area in our analysis, as its dust emissions are minor compared with those from the upwind arid and semi-arid sources.

Caution should be exercised when attributing dust emissions using local DOD measurements or direct image interpretation, as both methods are sensitive to surface reflectance, cloud cover, and threshold settings, which can lead to misidentifying transported dust as local emissions[64,65]. Our approach connects interannual variations in dust emissions within upwind source regions—considering their driving factors such as climate and surface conditions—with downwind DOD measurements. This strategy enables the detection of potential causal relationships and offers a physically grounded, spatially consistent framework suitable for large-scale analyses.

Climatic and vegetation products

We assembled a comprehensive set of variables based on dataset availability, including climate, vegetation, land use, and topography, to explore their potential impact on dust emissions (Supplementary Table 5). The higher precision of climate and vegetation products from ERA5-Land, AVHRR, and MODIS, compared to other reanalysis or observational data, helps reduce estimation bias caused by the strong spatial heterogeneity of dust emissions. Monthly climatic variables were derived from the ERA5-Land reanalysis dataset at a 0.1 × 0.1° spatial resolution[66]. Drought severity and duration were assessed using the Aridity Index (ratio between mean annual precipitation and mean annual reference evapo-transpiration) and the self-calibrating Palmer Drought Severity Index (scPDSI). Information for daily snow cover was derived from the AVHRR and MODIS sensors. AVHRR data for snow cover was produced by the Snow project of the European Space Agency (ESA) Climate Change Initiative (CCI)[67,68], with an original resolution of about 5 × 5 km. MODIS data for snow cover were derived from MOD10C1 with a resolution of 0.05°[69]. We optimized the two data sets using a daily gap-filling approach to reduce the interference of clouds[70].

Vegetation plays a critical biophysical role in regulating dust emissions. To capture this effect and ensure the robustness of statistical analyses, we used multiple vegetation structure and phenology indicators. Biweekly GIMMS NDVI3g data (1982–2015) were derived from AVHRR at a 1/12° resolution[71,72], and Terra MODIS NDVI data (2001–2023) were obtained from monthly MOD13A3 Version 6.1 at a 1 km resolution. PKU GIMMS NDVI data (version 1.2) provide global, spatiotemporally consistent NDVI data at the same spatiotemporal resolution as GIMMS NDVI3g, covering 1982–2022. These data were generated using biome-specific back-propagation neural network (BPNN) models that integrated the GIMMS NDVI3g product and 3.6 million high-quality global Landsat NDVI samples. To extend the temporal coverage to 2022, PKU GIMMS NDVI was consolidated with MODIS NDVI data (MOD13C1) using a pixel-by-pixel random-forest fusion method[73]. GIMMS LAI4g (1982–2020) is an LAI product that leverages the latest PKU GIMMS NDVI and Landsat LAI samples, correcting for satellite orbital drift and sensor degradation using BPNN models[74]. GLASS LAI (1982–2021) comprises datasets derived from AVHRR and MODIS data, offering long-term temporal coverage, high spatial resolution (1 km and 0.05°), spatial continuity without missing pixels, and validated accuracy through in situ measurements and satellite comparisons[75].

To assess the potential impact of vegetation seasonality on dust emissions, we derived green-up date (GUD) from the 16-day MODIS NDVI dataset (MOD13C1, 0.05° resolution). The use of biweekly NDVI data, as suggested in previous studies, does not bias the estimation of temporal changes in GUD or temperature sensitivity[76]. We first addressed the deviation in estimating phenology from NDVI time series due to annual variations in background values outside the growing season such as cloud, snow and aerosols (see Shen et al.[76] for specific methods). The Savitzky–Golay filter was used to denoise the NDVI time series. Two threshold methods were then used to define GUD, one based on 20% of the annual NDVI amplitude[77] and the other based on 20% of the relative NDVI amplitude for the entire time, which was calculated as the difference between the robust mean maximum level and the robust mean base level[78]. The outputs from the two methodologies were strongly correlated interannually. We thus used their means for statistical analysis to mitigate uncertainties. For more details and additional variables, please refer to Supplementary Table 5.

Land cover type and ecoregion datasets

Land-use–driven changes in land cover have substantially reshaped global vegetation patterns over recent decades[24]. To assess how land use changes influence vegetation and dust emissions, we used two long-term land cover datasets: MODIS (MCD12Q1, 500 m, Collection 6.1, 2001–2022) and ESA CCI (300 m, 1992–2020). Both datasets were reclassified into four broad biome types—barren, grasslands, croplands, and other—of which only the first three were used due to their dominance in dust source regions. Forests were excluded from the analysis because they are limited to localized mountainous areas

surrounding the dust source regions (Supplementary Fig. 12, gray-shaded region).

To inform region-specific dust mitigation strategies, we further examined differences among ecoregions using the 'Terrestrial Ecoregions of the World' dataset[79]. This map, maintained by UNEP-WCMC, integrates biodiversity and conservation priorities across global ecoregions. We excluded the Helanshan montane conifer forests, which contributed little to dust emission in Eastern Sources, and selected five other ecoregions for analysis, namely, Alashan Plateau semi-desert, Gobi Lakes Valley desert steppe, Eastern Gobi desert steppe, Mongolian-Manchurian grassland, and Ordos Plateau steppe. Within these ecoregions, we quantified three potential ecological factors influencing vegetation's role in dust emission. First, Water Limitation Index was assessed using the Pearson correlation between spring scPDSI and NDVI (MOD13A3) during 2001–2023, where positive values indicate drought-constrained vegetation growth[30] (Supplementary Fig. 13e). Second, grazing pressure was represented by the change in total livestock (cattle, sheep, and goats) between 2010 and 2020, based on available FAO statistics, which provide a consistent proxy for grazing intensity across ecoregions. Finally, dominant species and plant functional types in the Alashan Plateau were examined using the 1:1,000,000 Vegetation Map of China, highlighting the importance of perennial woody and semi-woody shrubs in shaping vegetation structure and influencing dust emissions from major source areas (Supplementary Table 2).

Model of dust emission

Quantifying dust emissions is essential for understanding and responding to their variability. Given the complex interplay of multiple factors influencing dust emission, statistical analyses alone face challenges in isolating these effects. Therefore, it is crucial to use numerical models that capture the non-linear impacts of relevant factors on dust particle dynamics in a physical manner[23]. To address this issue, we employed a physically based dust emission model (DuEM v1), developed by Wu et al.[23], which explicitly represents nonlinear responses of dust flux to surface wind speed, vegetation cover, soil moisture, and snow cover. Comparisons with field observations have demonstrated the reliability of the model[15,80], which has been extensively applied in regional[23,81–84] and global[85,86] models of dust. A comprehensive description of the model is provided in Supplementary Methods. In this study, we used the DuEM model to simulate dust emission at an hourly resolution over the last four decades and future scenarios.

The spatiotemporal reliabilities of the DuEM model have been verified using records of dust storms, MERRA-2 DOD data and satellite images across hourly to annual scales (Supplementary Figs. 8, 22–23). Compared with MERRA-2 outputs, DuEM dust emissions exhibited a finer spatial resolution of 0.25° × 0.25° and demonstrated higher simulation confidence, as interannual correlations with downwind dust storm days increased from $R^2 = 0.44$ (MERRA-2) to $R^2 = 0.55$ (DuEM) during 2001–2023 (Supplementary Fig. 23). We found that downwind DOD in regions affected by dust was more effective for model validation than was local DOD in Eastern Sources (Supplementary Fig. 23c). This finding further supports our use of downwind DOD as the dependent variable in our statistical analysis. Incorporating changes to vegetation notably increased the explainability of the frequency of dust storms and identified a more pronounced trend (Supplementary Fig. 8d).

Forcing data for the model of dust emission

The hourly forcing data, including the friction velocity, surface pressure and soil-moisture, were derived from the hourly data of the fifth generation ECMWF atmospheric reanalysis (ERA5) on single levels (surface or near-surface levels)[87]. Instantaneous two-dimensional fields were provided hourly at a spatial resolution of 0.25 × 0.25°. ERA5 began in 1940, but we used the data from 1982–2023. Vegetation cover data are constructed from GIMMS NDVI3g and MODIS NDVI data (MOD13C1) using the improved pixel bipartite model[88,89]. The two data sets are linearly interpolated to generate daily fields for the dust model (detailed in Supplementary Methods and Supplementary Table 6). We used the two vegetation products to drive the model, which exhibit high consistency for dust emission. In Phase 1, the model was driven by GIMMS vegetation cover data for 1982–2015, while in Phase 2, it was driven by MODIS vegetation cover data for 2001–2023 (Supplementary Fig. 8c). For projections of dust emissions under three shared socioeconomic pathways (SSP1-2.6, SSP2-4.5 and SSP5-8.5) outlined in the sixth phase of the Coupled Model Intercomparison Project (CMIP6, last accessed on 31 October 2023), we selected outputs from an ensemble of 12 CMIP6 models to drive our simulations (detailed in Supplementary Methods and Supplementary Table 7 and 8).

Statistical analyses

We re-gridded all relevant metrics to a spatial resolution of 0.05 × 0.05° before the analysis using cubic resampling. We calculated the spring (March to May) metrics due to the strong correlation between peak dust storms, such as those in Eastern Asia during spring, and annual dust levels. This correlation facilitated the use of spring dust metrics as a proxy for the annual quantities of dust, thus simplifying our statistical analysis. Based on the availability of high-quality data, we used data from the period 2001–2020 to detect and attribute interannual variations in dust emissions. Furthermore, we removed linear trends from the data using MATLAB's detrend function prior to analysis, enabling a more accurate examination of these fluctuations.

We used the random-forest algorithm[90] to rank these environmental factors based on their influence on the patterns of dust emission (assessed using spring average MERRA-2 dust emissions for 2001–2020). The random-forest algorithm is a nonparametric modeling technique capable of identifying nonlinearities and interactions among independent variables, without making any assumptions about the data[91]. A strength of the algorithm is that we do not need to specify aspects, such as the order of independent variables and their interactions, and the algorithm can identify inherent patterns and effectively avoid overfitting in a very large data set[92]. We implemented the above analysis using the 'randomForest' version 4.7-1.1 R package.

We selected eight key environmental factors based on random forests for conducting a partial correlation analysis. These eight factors can be categorized into wind, moisture (precipitation, snow cover and soil moisture), vegetation (NDVI, LAI and GUD) and temperature; we selected wind speed, soil moisture, NDVI and air temperature as representative controlling factors. We controlled for the representative factors of the other three categories when calculating the partial contribution of a particular factor.

We also investigated the environmental influence on key variables using a partial least-squares regression model (PLSR). In addition to the model coefficients, the PLSR model calculates variable importance (VIP), with its absolute value representing the importance of the factor to the interannual variability of spring dust emissions. The PLSR model has a 'greater than one'[93] criterion; a VIP value > 1 demonstrates that the driver has a large influence on dust emission[94]. We also evaluated how the importance of the filtered driving factors varied across environmental gradients, leveraging the strengths of the model, aiming to identify potential thresholds or tipping points imposed by environmental constraints. We implemented the above analysis using the 'pls' version 2.8-1 R package.

Wind-driven interannual variations in dust activity may be influenced by large-scale climate patterns through teleconnections[8]. To explore these potential connections, we obtained multiple climate indices from National Oceanic and Atmospheric Administration webpages (NOAA, https://www.cpc.ncep.noaa.gov/ and https://www.ncei.noaa.gov/access/monitoring/products/), including the Antarctic Oscillation (AAO), Atlantic Multidecadal Oscillation (AMO), Arctic

Oscillation (AO), El Niño-Southern Oscillation (ENSO, using the Niño 3.4 index), North Atlantic Oscillation (NAO), Pacific Decadal Oscillation (PDO), and the Pacific/North American (PNA) pattern, calculated following standard NOAA procedures. Pearson correlation analysis was conducted between spring-time MERRA-2 DOD downwind and these climate indices. We specifically examined these indices for both current and previous year's months to evaluate their influence on dust activity (Supplementary Fig. 7).

Path analysis

We developed a path analysis to better understand how vegetation affects dust activity based on previous research[95]. Predicted hypotheses were assigned a relative importance within a single-path diagram by decomposing bivariate correlation coefficients into path coefficients[96]. Based on our hypotheses, we built a path model for four indirect effect paths of vegetation on dust emission (Supplementary Fig. 14). Specifically, we examined how increased vegetation cover might reduce surface temperature, thus decreasing soil moisture loss and enhancing soil compaction; directly increase soil moisture, improving soil stability and resistance to wind erosion; enhance surface roughness, which lowers wind speed; and further reduce soil moisture evaporation through decreased wind speed, leading to greater soil compaction and erosion resistance.

We also considered the relative impacts of additional factors, including surface wind speed, temperature, precipitation and spring phenology, on the emission of dust to constrain our model outcomes. We used the 'piecewise-SEM' R package to execute our model in R v.4.2.2[97,98]. To determine the relative effects, we first excluded pixels with $P < 0.05$ (low fitness of the model) and then counted the standardized path coefficients of the remaining pixels[99]. Consistent with the previous statistical analysis, the model was executed using the detrended data from the period 2001–2020 to ensure a focus on interannual fluctuations in dust emissions.

Model experiments

We conducted four controlled experiments to isolate impacts of various factors (Supplementary Table 1).

Baseline: In the first experiment, we established a baseline by considering the variations in all variables, including friction velocity, vegetation cover, soil-moisture content and snow cover. This provided a reference point for understanding the combined effects of these factors on dust emission.

Experiment 1: For this experiment, we focused exclusively on the variations of the target variable and kept the remaining variables fixed at their values from the first year of the data series. Given the seasonal nature of dust emission, we accounted for intra-annual variations in these variables and excluded their interannual changes, as outlined by Wu et al.[23]. This helped us understand how specific variables drive dust emissions independently of long-term trends.

Experiment 2: In this experiment, we isolated the effect of vegetation by holding it constant at its values from the first year, while allowing other variables—such as friction velocity, soil moisture, and snow cover—to vary over time. Seasonal variations in vegetation were still included, so friction velocity could respond to seasonal vegetation structure. By comparing the results of this experiment with the baseline, where all factors were allowed to vary, we were able to quantify the specific contribution of vegetation to dust emissions. This approach strengthened the robustness of our results by clearly distinguishing the role of vegetation from other influencing factors.

Experiment 3: When a clear trend in dust emission is present, it becomes possible to quantify the contribution of each driving factor more effectively. We re-evaluated the primary drivers of changes to dust emission for 2001 to 2017 by incorporating refined observations and reanalysis metrics into the DuEM model, following the approach of Wu et al.[23]. The contribution of each driver to the variability of dust emission was quantified by isolating its effect between 2010 and 2017 and comparing it to its baseline level in 2001 (Fig. 3). Importantly, we used the term 'change' instead of 'decrease' because the impact of regional drivers on dust emissions can be either positive or negative.

Detection of dominant drivers of dust emissions at different timescales

To identify the dominant environmental drivers of future dust emissions under different climate scenarios, we applied two complementary approaches: correlation-based statistical analysis and Empirical Ensemble Mode Decomposition (EEMD).

Correlation-based driver attribution: We assessed statistical associations between dust emissions and three drivers—surface wind speed, FVC, and soil moisture—using Pearson and partial correlation analyses. To separate short-term variability from long-term trends, a 20-year Savitzky-Golay filter was applied to the dust time series. We then computed: (1) correlations between each unfiltered driver and unfiltered dust (Pearson-1), and (2) correlations between each driver and the smoothed dust trend (Pearson-2). Partial correlations were also calculated, controlling for the other two variables, to isolate each factor's unique effect. These analyses were conducted separately for each scenario, identifying drivers of both interannual and multidecadal dust variability (Fig. 4).

Empirical mode decomposition analysis: To further investigate the scale-dependent relationships between dust emissions and their drivers, we applied EEMD[100,101] using the Rlibeemd package in R (v4.4.1). EEMD decomposes a time series into a finite number of Intrinsic Mode Functions (IMFs), each representing oscillations at distinct timescales.

For each scenario, we applied EEMD to the annual dust emission time series using an ensemble size of 100 and a noise strength of 0.2 (relative to the standard deviation). The resulting IMFs were used to estimate their characteristic timescales based on zero-crossing analysis. We then computed the absolute Pearson correlation coefficients between each IMF and the original (unfiltered) time series of each driver (Wind, FVC, SoilM). This analysis allowed us to track how the influence of each factor evolved with increasing temporal scale (Supplementary Fig. 18).

Reporting summary

Further information on research design is available in the Nature Portfolio Reporting Summary linked to this article.

Data availability

The data generated in this study have been deposited in a public repository and are available via figshare at https://doi.org/10.6084/m9.figshare.29652356.v3 (ref. 102.), with a backup copy hosted at https://doi.org/10.11888/Terre.tpdc.301534. The data used in this study are publicly available from third-party sources, including MERRA-2 data: https://disc.sci.gsfc.nasa.gov/datasets/; ERA5-Land monthly data: https://cds.climate.copernicus.eu/datasets/reanalysis-era5-land-monthly-means?tab=overview; ERA5 hourly data: https://cds.climate.copernicus.eu/datasets/reanalysis-era5-single-levels?tab=overview; Dust storm records: https://www.ncei.noaa.gov/pub/data/noaa/ and https://doi.org/10.57760/sciencedb.03301 CMIP6 data: https://aims2.llnl.gov/search/cmip6/; NEX-GDDP-CMIP6 downscaled data: https://nex-gddp-cmip6.s3.us-west-2.amazonaws.com/index.html#NEX-GDDP-CMIP6/; Population data: https://hub.worldpop.org/; Human footprint data: https://www.x-mol.com/groups/li_xuecao/news/48145; Nighttime light data: https://eogdata.mines.edu/products/vnl/; ESA-CCI land cover: https://maps.elie.ucl.ac.be/CCI/viewer/; FAO livestock data: https://www.fao.org/livestock-systems/global-distributions/en/; Climate indices: https://www.cpc.ncep.noaa.gov/ and https://www.ncei.noaa.gov/access/monitoring/products/. Additional publicly

available climate and vegetation datasets are listed with detailed access links and descriptions in Supplementary Table 5.

Code availability

All data analyses were performed using MATLAB or R. The code for the dust emission model is available in the Supplementary Software provided by Wu et al.[23], and can be accessed via https://doi.org/10.1038/s41467-022-34823-3. Other codes required to reproduce the results and figures presented in the main text have been deposited at https://doi.org/10.6084/m9.figshare.29652356.v3 (ref. 102).

References

1. United Nations Economic and Social Commission for Asia and the Pacific (ESCAP). *Sand and dust storms in Asia and the Pacific: opportunities for regional cooperation and action* (United Nations Economic and Social Commission for Asia and the Pacific, Bangkok, 2018).
2. Heft-Neal, S. et al. Dust pollution from the Sahara and African infant mortality. *Nat. Sustain.* **3**, 863–871 (2020).
3. Zhang, C. et al. Mortality risks from a spectrum of causes associated with sand and dust storms in China. *Nat. Commun.* **14**, 6867 (2023).
4. Tegen, I., Werner, M., Harrison, S. P. & Kohfeld, K. E. Relative importance of climate and land use in determining present and future global soil dust emission. *Geophys. Res. Lett.* **31**, L05105 (2004).
5. Ravi, S. et al. Aeolian processes and the biosphere. *Rev. Geophys.* **49**, RG3001 (2011).
6. Kok, J. F. et al. Mineral dust aerosol impacts on global climate and climate change. *Nat. Rev. Earth Environ.* **4**, 71–86 (2023).
7. Kwon, H.-J., Cho, S.-H., Chun, Y., Lagarde, F. & Pershagen, G. Effects of the Asian dust events on daily mortality in Seoul, Korea. *Environ. Res.* **90**, 1–5 (2002).
8. Shao, Y., Klose, M. & Wyrwoll, K. H. Recent global dust trend and connections to climate forcing. *J. Geophys. Res.-Atmos.* **118**, 11107–11108 (2013).
9. Tai, A. P. K. et al. Impacts of climate and land cover variability and trends on springtime East Asian dust emission over 1982–2010: a modeling study. *Atmos. Environ.* **254**, 118348 (2021).
10. Musick, H. B. & Gillette, D. A. Field evaluation of relationships between a vegetation structural parameter and sheltering against wind erosion. *Land Degrad. Dev.* **2**, 87–94 (2006).
11. Adebiyi, A. A. et al. Fallowed agricultural lands dominate anthropogenic dust sources in California. *Commun. Earth Environ.* **6**, 324 (2025).
12. Piao, S. et al. Socioeconomic and Environmental Changes in Global Drylands. in *Dryland Social-Ecological Systems in Changing Environments* (Fu, B., Stafford-Smith, M. eds) (Springer, Singapore, 2024).
13. Gillette, D. Environmental factors affecting dust emission by wind erosion. in *Saharan Dust*, (Morales, C. ed) 71–94, (John Wiley, Hoboken, 1979).
14. Marticorena, B. & Bergametti, G. Modeling the atmospheric dust cycle: 1. Design of a soil-derived dust emission scheme. *J. Geophys. Res.-Atmos* **100**, 16415–16430 (1995).
15. Shao, Y. Simplification of a dust emission scheme and comparison with data. *J. Geophys. Res.-Atmos.* **109**, D10202 (2004).
16. Shao, Y. et al. Dust cycle: an emerging core theme in Earth system science. *Aeolian Res.* **2**, 181–204 (2011).
17. Muhs, D. R. The geologic records of dust in the Quaternary. *Aeolian Res.* **9**, 3–48 (2013).
18. Neff, J. C. et al. Increasing eolian dust deposition in the western United States linked to human activity. *Nat. Geosci.* **1**, 189–195 (2008).
19. Piao, J. et al. Increased sandstorm frequency in North China in 2023: climate change reflection on the Mongolian plateau. *Innovation* **4**, 100497 (2023).
20. Yin, Z., Wan, Y., Zhang, Y. & Wang, H. Why super sandstorm 2021 in North China? *Natl. Sci. Rev.* **9**, nwab165 (2022).
21. Mulitza, S. et al. Increase in African dust flux at the onset of commercial agriculture in the Sahel region. *Nature* **466**, 226–228 (2010).
22. Chen, F. et al. Asian dust-storm activity dominated by Chinese dynasty changes since 2000 BP. *Nat. Commun.* **11**, 992 (2020).
23. Wu, C., Lin, Z., Shao, Y., Liu, X. & Li, Y. Drivers of recent decline in dust activity over East Asia. *Nat. Commun.* **13**, 7105 (2022).
24. Chen, C. et al. China and India lead in greening of the world through land-use management. *Nat. Sustain.* **2**, 122–129 (2019).
25. Chen, S. et al. Mongolia contributed more than 42% of the dust concentrations in northern China in march and april 2023. *Adv. Atmos. Sci.* **40**, 1549–1557 (2023).
26. Wang, B., Wu, R. & Fu, X. Pacific–East Asian teleconnection: how does ENSO affect East Asian climate? *J. Climate* **13**, 1517–1536 (2000).
27. Wang, L., Chen, W. & Huang, R. Interdecadal modulation of PDO on the impact of ENSO on the east Asian winter monsoon. *Geophys. Res. Lett.* **35**, L20702 (2008).
28. Nakamura, T. et al. A negative phase shift of the winter AO/NAO due to the recent Arctic sea-ice reduction in late autumn. *J. Geophys. Res. Atmos.* **120**, 3209–3227 (2015).
29. Tariq, A. et al. Guardians of arid lands: deep-rooted defense against desertification and climate change. *Trends Plant Sci*. (in press), https://doi.org/10.1016/j.tplants.2025.10.009 (2025).
30. Jiao, W. et al. Observed increasing water constraint on vegetation growth over the last three decades. *Nat. Commun.* **12**, 3777 (2021).
31. Shinoda, M., Gillies, J. A., Mikami, M. & Shao, Y. Temperate grasslands as a dust source: Knowledge, uncertainties, and challenges. *Aeolian Res.* **3**, 271–293 (2011).
32. Forzieri, G., Dakos, V., McDowell, N. G., Ramdane, A. & Cescatti, A. Emerging signals of declining forest resilience under climate change. *Nature* **608**, 534–539 (2022).
33. Zhu, Z. et al. Greening of the Earth and its drivers. *Nat. Clim. Change* **6**, 791–795 (2016).
34. Piao, S. et al. Characteristics, drivers and feedbacks of global greening. *Nat. Rev. Earth Environ.* **1**, 14–27 (2019).
35. Wang, S. et al. Reduced sediment transport in the Yellow River due to anthropogenic changes. *Nat. Geosci.* **9**, 38–41 (2016).
36. Lian, X. et al. Multifaceted characteristics of dryland aridity changes in a warming world. *Nat. Rev. Earth Environ.* **2**, 232–250 (2021).
37. Wang, X. et al. Desert ecosystems in China: past, present, and future. *Earth-Sci. Rev.* **234**, 104206 (2022).
38. Zhang, X. et al. Fading regulation of diurnal temperature ranges on drought-induced growth loss for drought-tolerant tree species. *Nat. Commun.* **14**, 6916 (2023).
39. Ru, J. et al. Advanced precipitation peak offsets middle growing-season drought in impacting grassland C sink. *New Phytol* **244**, 1775–1787 (2024).
40. Cheng, Y. & Liu, H. The crucial role of soil moisture in the evolution of forest cover in Asia since the Last Glacial Maximum. *Innovation* **5**, 10594 (2024).
41. Shao, Y. Adhesion theory and model for air humidity impact on dust emission. *Aeolian Res.* **66**, 100898 (2024).
42. Fan, B. et al. Earlier vegetation green-up has reduced spring dust storms. *Sci. Rep.* **4**, 6749 (2014).
43. Hessl, A. E. et al. Past and future drought in Mongolia. *Sci. Adv.* **4**, e1701832 (2018).

44. Zhang, P. et al. Abrupt shift to hotter and drier climate over inner East Asia beyond the tipping point. *Science* **370**, 1095–1099 (2020).
45. Hauck, M., Klinge, M., Erasmi, S. & Dulamsuren, C. No signs of long-term greening trend in western Mongolian grasslands. *Ecosystems* **26**, 1125–1143 (2023).
46. D'Odorico, P., Bhattachan, A., Davis, K. F., Ravi, S. & Runyan, C. W. Global desertification: drivers and feedbacks. *Adv. Water Resour.* **51**, 326–344 (2013).
47. Liu, J. et al. Dust storms in northern China and their significance for the concept of the Anthropocene. *Sci. China Earth Sci.* **65**, 921–933 (2022).
48. Song, J. et al. Ecological restoration enhances dryland carbon stock by reducing surface soil carbon loss due to wind erosion. *Proc. Natl. Acad. Sci. USA.* **121**, e2416281121 (2024).
49. Zhan, W. et al. Reduced water loss rather than increased photosynthesis controls CO2-enhanced water-use efficiency. *Nat. Ecol. Evol.* **9**, 1571–1584 (2025).
50. Diffenbaugh, N. S., Swain, D. L. & Touma, D. Anthropogenic warming has increased drought risk in California. *Proc. Natl. Acad. Sci. USA.* **112**, 3931–3936 (2015).
51. Pryor, S. C., Barthelmie, R. J., Bukovsky, M. S., Leung, L. R. & Sakaguchi, K. Climate change impacts on wind power generation. *Nat. Rev. Earth Environ.* **1**, 627–643 (2020).
52. Zhang, X. et al. A large but transient carbon sink from urbanization and rural depopulation in China. *Nat. Sustain.* **5**, 321–328 (2022).
53. Zhang, S. et al. Photovoltaic systems promote grassland restoration by coordinating water and nutrient uptake, transport and utilization. *J. Clean. Prod.* **447**, 141437 (2024).
54. Okin, G. S. et al. Do changes in connectivity explain desertification? *BioScience* **59**, 237–244 (2009).
55. Lal, R. Soil degradation by erosion. *Land Degrad. Dev.* **12**, 519–539 (2001).
56. Reynolds, J. F. et al. Global desertification: building a science for dryland development. *Science* **316**, 847–851 (2007).
57. Xing, Q. et al. Intranational synergies and trade-offs reveal common and differentiated priorities of sustainable development goals in China. *Nat. Commun.* **15**, 2251 (2024).
58. Wu, J. et al. Estimation of dry vegetation cover and mass from MODIS data: verification by roughness length and sand saltation threshold. *Int. J. Appl. Earth Obs. Geoinf.* **102**, 102417 (2021).
59. Wu, J., Kurosaki, Y., Sekiyama, T. T. & Maki, T. Effects of dry vegetation coverage estimated from the MODIS Soil Tillage Index on dust occurrence: verification by surface synoptic observations. *J. Meteorol. Soc. Jpn. Ser. II* **101**, 67–77 (2023).
60. Buchard, V. et al. The MERRA-2 aerosol reanalysis, 1980 onward. Part II: Evaluation and case studies. *J. Clim.* **30**, 6851–6872 (2017).
61. Randles, C. A. et al. The MERRA-2 Aerosol Reanalysis, 1980 onward. Part I: System description and data assimilation evaluation. *J. Clim.* **30**, 6823–6850 (2017).
62. Zhu, Q., Liu, Y. & Xiao, N. The frequency and intensity of extreme dust events and related driving factors in major dust sources based on MERRA-2 aerosol reanalysis. *J. Clim.* **38**, 4491–4504 (2025).
63. Cui, J. et al. Global water availability boosted by vegetation-driven changes in atmospheric moisture transport. *Nat. Geosci.* **15**, 982–988 (2022).
64. Baddock, M. C., Bullard, J. E. & Bryant, R. G. Dust source identification using MODIS: A comparison of techniques applied to the Lake Eyre Basin, Australia. *Remote Sens. Environ.* **113**, 1511–1528 (2009).
65. Darvishi Boloorani, A. et al. Visual interpretation of satellite imagery for hotspot dust sources identification. *Remote Sens. Appl. Soc. Environ.* **29**, 100888 (2023).
66. Muñoz-Sabater, J. ERA5-Land monthly averaged data from 1950 to present. *Copernicus Clim. Change Service (C3S) Climate Data Store (CDS)* https://doi.org/10.24381/cds.68d2bb30 (2019).
67. Naegeli, K. et al. Revealing four decades of snow cover dynamics in the Hindu Kush Himalaya. *Sci. Rep.* **12**, 13443 (2022).
68. Naegeli, K. et al. ESA Snow Climate Change Initiative (Snow_cci): Daily global Snow Cover Fraction - snow on ground (SCFG) from AVHRR (1982–2018), version 2.0. *NERC EDS Centre for Environmental Data Analysis* https://doi.org/10.5285/3f034f4a08854eb59d58e1fa92d207b6 (2022).
69. Hall, D. K., Riggs, G. A., Foster, J. L. & Kumar, S. V. Development and evaluation of a cloud-gap-filled MODIS daily snow-cover product. *Remote Sens. Environ.* **114**, 496–503 (2010).
70. Foppa, N. & Seiz, G. Inter-annual variations of snow days over Switzerland from 2000–2010 derived from MODIS satellite data. *Cryosphere* **6**, 331–342 (2012).
71. Pinzon, J. E. & Tucker, C. J. A non-stationary 1981–2012 AVHRR NDVI3g time series. *Remote Sens* **6**, 6929–6960 (2014).
72. Tucker, C. J. et al. An extended AVHRR 8-km NDVI dataset compatible with MODIS and SPOT vegetation NDVI data. *Int. J. Remote Sens.* **26**, 4485–4498 (2005).
73. Li, M. et al. Spatiotemporally consistent global dataset of the GIMMS Normalized Difference Vegetation Index (PKU GIMMS NDVI) from 1982 to 2022. *Earth Syst. Sci. Data* **15**, 4181–4203 (2023).
74. Cao, S. et al. Spatiotemporally consistent global dataset of the GIMMS leaf area index (GIMMS LAI4g) from 1982 to 2020. *Earth Syst. Sci. Data* **15**, 4877–4899 (2023).
75. Liang, S. et al. The Global LAnd Surface Satellite (GLASS) products suite. *Bull. Amer. Meteor. Soc.* **102**, E323–E337 (2020).
76. Shen, M. et al. Greater temperature sensitivity of vegetation greenup onset date in areas with weaker temperature seasonality across the Northern Hemisphere. *Agr. Forest Meteorol.* **313**, 108759 (2022).
77. Yu, H., Luedeling, E. & Xu, J. Winter and spring warming result in delayed spring phenology on the Tibetan Plateau. *Proc. Natl. Acad. Sci. USA.* **107**, 22151–22156 (2010).
78. Jönsson, P. & Eklundh, L. Seasonality extraction and noise removal by function fitting to time-series of satellite sensor data. *IEEE T. Geosci. Remote* **40**, 1824–1832 (2002).
79. Dinerstein, E. et al. An ecoregion-based approach to protecting half the terrestrial realm. *Bioscience* **67**, 534–545 (2017).
80. Shao, Y., Ishizuka, M., Mikami, M. & Leys, J. F. Parameterization of size-resolved dust emission and validation with measurements. *J. Geophys. Res.-Atmos* **116**, D08203 (2011).
81. Shao, Y., Leys, J. F., McTainsh, G. H. & Tews, K. Numerical simulation of the October 2002 dust event in Australia. *J. Geophys. Res.-Atmos* **112**, D08207 (2007).
82. Shao, Y., Fink, A. H. & Klose, M. Numerical simulation of a continental-scale Saharan dust event. *J. Geophys. Res.-Atmos* **115**, D13205 (2010).
83. Kang, J. Y., Yoon, S. C., Shao, Y. & Kim, S. W. Comparison of vertical dust flux by implementing three dust emission schemes in WRF/Chem. *J. Geophys. Res.-Atmos* **116**, D09202 (2011).
84. Hamidi, M., Kavianpour, M. R. & Shao, Y. Numerical simulation of dust events in the Middle East. *Aeolian Res* **13**, 59–70 (2014).
85. Wu, C. et al. Description of dust emission parameterization in CASESM2 and its simulation of global dust cycle and East Asian dust events. *J. Adv. Modeling Earth Syst.* **13**, e2020MS002456 (2021).
86. Klose, M. et al. Mineral dust cycle in the Multiscale Online Nonhydrostatic AtmospheRe CHemistry model (MONARCH) Version 2.0. *Geosci. Model Dev.* **14**, 6403–6444 (2021).

87. Hersbach, H. et al. ERA5 hourly data on single levels from 1940 to present. *Copernicus Climate Change Service (C3S) Climate Data Store (CDS)* https://doi.org/10.24381/cds.adbb2d47 (2018).
88. Gutman, G. & Ignatov, A. The derivation of the green vegetation fraction from NOAA/AVHRR data for use in numerical weather prediction models. *Int. J. Remote Sens.* **19**, 1533–1543 (1998).
89. Rundquist, B. The influence of canopy green vegetation fraction on spectral measurements over native tallgrass prairie. *Remote Sens. Environ.* **8**, 129–135 (2002).
90. Strobl, C., Boulesteix, A. L., Kneib, T., Augustin, T. & Zeileis, A. Conditional variable importance for random forests. *BMC Bioinform* **9**, 1–11 (2008).
91. Breiman, L. Random forests. *Mach. Learn.* **45**, 5–32 (2001).
92. Wang, X. et al. Enhanced habitat loss of the Himalayan endemic flora driven by warming-forced upslope tree expansion. *Nat. Ecol. Evol.* **6**, 890–899 (2022).
93. Wold, S. PLS for multivariate linear modeling. *Chemom. Methods Mol. Des.* **195**, 218 (1995).
94. Guo, M., Wu, C., Peng, J., Lu, L. & Li, S. Identifying contributions of climatic and atmospheric changes to autumn phenology over mid-high latitudes of Northern Hemisphere. *Global Planet. Change* **197**, 103396 (2021).
95. Streiner, D. L. Finding our way: an introduction to path analysis. *Can. J. Psychiatry* **50**, 115–122 (2005).
96. Gao, S. et al. An earlier start of the thermal growing season enhances tree growth in cold humid areas but not in dry areas. *Nat. Ecol. Evol.* **6**, 397–404 (2022).
97. Lefcheck, J. piecewiseSEM: piecewise structural equation modelling in r for ecology, evolution, and systematics. *Methods Ecol. Evol.* **7**, 573–579 (2016).
98. R. Core Team. R. A language and environment for statistical computing. R Foundation for Statistical Computing, Vienna, Austria (2022). Available at: https://www.R-project.org/.
99. Dong, L., Wu, C., Wang, X. & Zhao, N. Satellite observed delaying effects of increased winds on spring green-up dates. *Remote Sens. Environ.* **284**, 113363 (2023).
100. Huang, N. E. et al. The empirical mode decomposition and the Hilbert spectrum for nonlinear and non-stationary time series analysis. *Proc. R. Soc. Lond. A Math. Phys. Eng. Sci.* **454**, 903–995 (1998).
101. Wu, Z. & Huang, N. E. Ensemble empirical mode decomposition: a noise-assisted data analysis method. *Adv. Adapt. Data Anal.* **1**, 1–41 (2009).
102. Fu, Y., Liang, E. & Wang, Y. Dust emission simulations over East Asia. *figshare* https://doi.org/10.6084/m9.figshare.29652356.v3 (2025).

Acknowledgements

This study was supported by the National Natural Science Foundation of China (U2243204, 42271003) and the State Scholarship Fund (202310550002) provided by the China Scholarship Council. C. Wu is supported by the National Large Scientific and Technological Infrastructure "Earth System Numerical Simulation Facility" (https://cstr.cn/31134.02.EL).

Author contributions

E.Y.L., Y.F.W., and S.L.P. led the concept development and writing. Y.F., C.L.W., and J.T.Z. conceived and designed the model and experiments. Y.F. performed the initial simulation, data curation, data analysis, visualization, and drafted the manuscript. C.L.W. provided the field data used to evaluate the model. S.G., J.P., and J.J.C. contributed to the concept and writing. D.L., X.Y.Z., and Z.L.L. contributed to writing and discussion. All authors reviewed and approved the manuscript.

Competing interests

The authors declare no competing interests.

Additional information

Supplementary information The online version contains supplementary material available at https://doi.org/10.1038/s41467-026-68427-y.

Correspondence and requests for materials should be addressed to Yafeng Wang.

Peer review information *Nature Communications* thanks Caroline Pierre, who co-reviewed with Paul-Alain Raynal, and Ali Darvishi Boloorani for their contribution to the peer review of this work. A peer review file is available.